Received: 7 April 2021 | Accepted: 12 April 2021

DOI: 10.1111/ppa.13392

Plant Pathology WILEY

ORIGINAL ARTICLE

The role of photoprotection in defence of two wheat genotypes against *Zymoseptoria tritici*

Olubukola O. Ajigboye[1] | **Dasuni P. Jayaweera**[1] | **Dimitra Angelopoulou**[1] | **Alexander V. Ruban**[2] | **Erik H. Murchie**[1] | **Victoria Pastor**[3] | **Richard Summers**[4] | **Rumiana V. Ray**[1]

[1]Division of Plant and Crop Sciences, School of Biosciences, University of Nottingham, Loughborough, UK

[2]School of Biological and Chemical Sciences, Queen Mary, University of London, London, UK

[3]Associated Unit EEZ-UJI, Metabolic Integration and Cell Signaling Laboratory, Plant Physiology Section, Universitat Jaume I, Associated Unit to the CSIC, Castellón de la Plana, Castellón, Spain

[4]Cereal Breeding and Research, RAGT Seeds, Ickleton, UK

Correspondence
Rumiana V. Ray, Division of Plant and Crop Sciences, School of Biosciences, University of Nottingham, Sutton Bonington, Loughborough, LE12 5RD, UK.
Email: rumiana.ray@nottingham.ac.uk

Funding information
Biotechnology and Biological Sciences Research Council, Grant/Award Number: BB/M011550/1; Innovate UK, Grant/Award Number: 38936-273309

Abstract

This study provides new insights into the role of photoprotection in preformed and induced defence of two wheat genotypes with contrasting phenotypes to infection by *Zymoseptoria tritici*. We investigated the mechanisms of the photoprotective response during early infection, including nonphotochemical quenching (NPQ), β-carotene-derived xanthophylls, reactive oxygen species, and the phytohormones abscisic acid (ABA), jasmonic acid (JA), and salicylic acid (SA). Furthermore, we quantified the effects of pathogenesis on photosynthesis, stomatal control, and expression of plant defence molecular markers. The photoprotective mechanism of successful defence involved the qI component of NPQ leading to rapid down-regulation of photosystem II quantum yield and chlorophyll *a*:*b*, increased biosynthesis of the xanthophyll neoxanthin and ABA, and the expression of chloroplast-specific enzymes to engage in scavenging of $O_2^{\bullet-}$. Elevated ABA in the resistant genotype correlated with preformed leaf defence traits including low stomatal density, increased expression of wax biosynthesis, and lignification. *Z. tritici* exhibited reduced germination and branching on the resistant host genotype and hijacked stomatal control in both genotypes by enhancing stomatal sensitivity to light. Increased biosynthesis of JA and anthocyanins, in contrast to SA, were quantified in the incompatible interaction. Our results indicate that ABA and JA in antagonistic action to SA were associated with defence in the resistant genotype, Cougar, against *Z. tritici*.

KEYWORDS
photoprotection, phytohormones, reactive oxygen species (ROS), stomatal conductance, xanthophylls, *Zymoseptoria tritici*

1 | INTRODUCTION

Zymoseptoria tritici is one of the most important fungal pathogens of wheat causing Septoria tritici blotch (STB). *Z. tritici* is considered a latent necrotroph because of a symptomless phase of host invasion during which the pathogen does not acquire nutrition from the host but instead uses its own stored energy (Rudd et al., 2015). The infection process involves the transition of the germinating ascospore or pycnidiospore upon contact with the leaf into hyphal growth to facilitate penetration of substomatal cavities, followed by invasion of the

intercellular space before colonization of the apoplast (Kema et al., 1996). Thereafter, triggered by an unknown signal, pathogenesis transitions into a necrotrophic phase resulting in plant cell death before completion of the reproductive cycle of *Z. tritici* with the development of pycnidia in adjacent substomatal cavities (Shetty et al., 2003). The morphology, function, and density of the stomata as the main entry point for *Z. tritici* are therefore important traits in preformed host defence to infection and colonization (Tateda et al., 2019). Furthermore, as the pathogen has low expression of genes encoding cutinases to degrade leaf cutin (Kema et al., 1996) and is unable to penetrate the host directly (Shetty et al., 2003), leaf characteristics such as increased cuticle wax synthesis and deposition, interfering with the ability of a pathogen to physically locate the stomata (Rubiales & Niks, 1996), are likely to contribute significantly to passive resistance.

Early pathogen recognition perceived in the apoplast triggers the accumulation of hydrogen peroxide (H_2O_2) in the chloroplast required for the initiation of the hypersensitive response (HR) that is a form of programmed cell death (PCD; Serrano et al., 2016). Thus, the chloroplast is considered crucial in mediating host–pathogen interactions, including those of *Z. tritici* and wheat (Lee et al., 2015). Silencing two key chloroplast genes involved in the carotenoid and chlorophyll biosynthesis, phytoene desaturase and Mg-chelatase H subunit, respectively, rendered *Stb6*-mediated resistance in wheat to *Z. tritici* partially compromised; this resulted in increased susceptibility and PCD associated with excessive superoxide and hydrogen peroxide accumulation (Lee et al., 2015). These results strongly suggest that the inability of the host to regulate oxidative stress via the chloroplast is probably exploited by the pathogen to overcome host defence. The chloroplast itself is a major source of reactive oxygen species (ROS), which are largely nondamaging due to high redox regulation by the plant (Foyer & Noctor, 2005). However, pathogenesis associated with continuous ROS formation from excessive excitation energy due to over-reductions of the photosynthetic electron transport chain increases the imbalance in the chloroplast redox state and induces oxidative stress leading to photodamage in leaves (Triantaphylidès et al., 2008). Plants possess photoprotective mechanisms to protect the integrity of the photosynthetic apparatus and regulate ROS and one such major mechanism is thermal dissipation of excess excitation energy within light harvesting complexes of photosystem II (PSII) via nonphotochemical quenching (NPQ) (Murchie & Ruban, 2020). The major component of NPQ is the fast-relaxing, energy quenching (qE) form, regulated by the protein PsbS and zeaxanthin in the xanthophyll cycle (Ruban, 2016), whilst the slow-relaxing component of NPQ, photoinhibitory quenching (qI), is associated with a combination of photoinhibition of PSII and photoprotection (Demmig-Adams & Adams, 2006). Zeaxanthin, which also plays a part in qI (Demmig-Adams & Adams, 2006), is the first precursor of abscisic acid (ABA). Under low light and alkaline conditions, it is converted via zeaxanthin epoxidase into violaxanthin, followed by violaxanthin conversion to neoxanthin and xanthoxin through a series of isomerization reactions, and a deoxygenation step by 9-*cis*-epoxycarotenoid dioxygenase (NCED) cleaves xanthoxin from the C_{40} carotenoid (Ton et al., 2009). Conversely, under high light and low pH, the enzyme violaxanthin de-epoxidase converts violaxanthin into zeaxanthin in the xanthophyll cycle using ascorbate as a reductant and thus antagonizing ABA synthesis (Pastori et al., 2003). ABA regulates stomatal development, patterning, and function and mediates the properties of the wax cuticle in plants (Chater et al., 2014). Furthermore, ABA modulates salicylic (SA) and jasmonic acid (JA) signalling during the early and later resistance to pathogen penetration, promoting early defence against infection by enhancing JA-dependent defence and inhibiting SA-dependent signalling and ROS (Ton et al., 2009). Formed ROS are typically regulated through detoxification via multiple enzymes and nonenzymatic antioxidants to effectively return them to basal levels (Foyer & Noctor, 2005). Enzymatic antioxidants include superoxide dismutases (SODs), catalase (CAT), ascorbate peroxidase (APX), and glutathione peroxidase (GPX) involved in the conversion of $O_2^{\bullet-}$, generated at photosystem I (PSI), to H_2O_2 and further reduction to H_2O (Foyer & Noctor, 2005). However, the most potent physical scavengers of ROS are the carotenoids and the anthocyanins; the latter are typically stimulated by JA, initially formed via lipid peroxidation caused by singlet oxygen ($^1O_2$) in the chloroplast (Demmig-Adams et al., 2013). Previous studies have shown that changes in NPQ during pathogen attack can be related to immune responses of plants; however, the role of photoprotection in host defence against *Z. tritici* has not been investigated.

In this study, we aimed to elucidate the photoprotective mechanisms in the chloroplast that are involved in the defence response of wheat to *Z. tritici* during early disease development. We chose to investigate the responses of two wheat cultivars, Cougar and Sacramento, because of their contrasting disease phenotypes. STB resistance in Cougar is characterized by the lack of HR, delayed symptom expression, and impaired pathogen reproduction, whilst Sacramento shows HR coupled with rapid necrosis and formation of pycnidia. We hypothesized that, in Cougar, there is a limited formation or enhanced detoxification of ROS associated with changes in NPQ, consistent with an increased role of xanthophylls and antioxidants in the chloroplast. To determine how *Z. tritici* affects NPQ components, we analysed NPQ induction and relaxation kinetics at 24 hr postinoculation (hpi). We defined the behaviour of *Z. tritici* during the infection process using in vitro assays and microscopic observations, visualized ROS, and investigated the mechanisms of detoxification. We quantified changes in β-carotene-derived xanthophylls and ABA, and the phytohormones JA and SA, and explored the quantitative expression of key defence molecular markers during infection. Finally, we characterized the physiology of responses during the transition to the symptomatic phase of the disease to show the effects of compatible and incompatible interactions on stomatal conductance, photosynthesis, and chlorophyll fluorescence.

2 | MATERIALS AND METHODS

2.1 | Plant material and growth conditions

Z. tritici-resistant wheat (*Triticum aestivum*) cultivar Cougar and the susceptible cultivar Sacramento used in this study were provided by RAGT, UK. Plants were grown in a controlled-environment growth

room at a day:night temperature of 20:17 °C, 12 hr photoperiod and light intensity of 350 µmol·m^{-2}·s^{-1}. All measurements and leaf sampling were carried out at the growth stage GS23. In "dark" experiments, plants were kept in darkness for 24 hr before and after inoculation. All experiments except herbicide treatment (three replicates) were repeated at least twice with four to nine replicates.

2.2 | Inoculum preparation, inoculation procedure, and disease assessment

Z. tritici isolate ROY-UN was obtained from Dr Stephen Rossall, University of Nottingham, UK. The isolate, which had been stored at −80 °C, was grown on potato dextrose agar (PDA; Sigma) for 3 days at 22 °C and a fungal spore suspension of 10^6 spores/ml was prepared. Plants were spray inoculated with the spore suspension until runoff and then kept under high humidity for 48 hpi to encourage disease development. Bags were removed before measurements or sampling. In the dark experiments, inoculation was carried out in dim light of c.3 µmol·m^{-2}·s^{-1} and plants remained in darkness until sampling. Disease severity was visually estimated as leaf area covered by chlorotic and necrotic lesions relative to the whole leaf area and expressed as percentage leaf surface area exhibiting STB symptoms. To demonstrate active resistance, leaves were infiltrated with *Z. tritici* conidiospores (10^6 spores/ml) and kept under high humidity for 48 hr to encourage disease development. Images of chlorotic and necrotic lesions were measured with ImageJ software (https://imagej.nih.gov/ij/).

2.3 | Hyphal and stomatal observations, histochemical staining, H_2O_2 quantification, and ion leakage assays

A full list of references for the published protocols used in this section is shown in Table S1. In spore germination assays, 10 µl spore suspension (10^6 spores/ml) was placed on each of five 1 cm^2 pieces of leaf tissue; these were incubated in darkness at 20 °C and subsequently fixed in 10 µl lactophenol blue. Fungal structures were stained using trypan blue and analysed as described by Shetty et al. (2003). Total hyphal length (mm), germ tube extension (µm), and hyphal branching were measured using ImageJ software. To show lignin accumulation, leaf samples harvested at 2, 5, and 21 days after inoculation were cleared using ethanol:acetic acid as described by Shetty et al. (2003). Lignin was detected in the cleared leaf samples using toluidine blue O.

Stomatal length (mm), width (mm), and leaf stomatal density expressed as the number of stomata per unit leaf area (mm^2) were assessed on the adaxial leaf surface using impressions made with clear nail vanish. Imprints were made on the middle area of the leaf between the leaf base and tip of the youngest fully expanded leaf on the main tiller with three replications per genotype. The imprints were peeled off from the leaf surface, mounted on a microscope slide, and were imaged using a CTR 5000 light microscope (Leica Microsystems) using 10× magnification. A total of 20 non-overlapping images were taken per genotype. Stomatal length and width were measured using ImageJ software.

Histochemical staining of hydrogen peroxide (H_2O_2) was carried out using 3,3′-diaminobenzidine (DAB). Leaf sections were vacuum-infiltrated with 1 mg/ml DAB-HCl (pH 3.8) and incubated for 24 hr with gentle shaking at room temperature. The DAB solution was removed, and the leaf sections were washed with distilled water. To stop the reaction and fix the tissue, samples were boiled for 5 min in 95% ethanol.

Generation of superoxide anion ($O_2^{\bullet-}$) in leaves was detected in situ with nitroblue tetrazolium (NBT) with the addition of sodium azide. Leaf sections were vacuum infiltrated with 50 mM phosphate buffer (pH 7.8) containing 0.1% NBT and 10 mM sodium azide at different time points and incubated at room temperature for 1 hr with gentle shaking in darkness. Subsequently, chlorophyll was removed by boiling for 5 min in 95% ethanol. Leaves were preserved at room temperature in 95% ethanol.

For both $O_2^{\bullet-}$ and H_2O_2 staining, leaf sections were sampled in three replications from fully expanded leaves on the main tiller; these were harvested prior to inoculation (0 hr) and at 8 and 24 hpi with *Z. tritici* conidiospores. This assay was repeated in three independent experiments. After staining, DAB and NBT stained samples were imaged using a Nikon D600 DSLR camera. Production of H_2O_2 was assayed using the reagents and protocols provided in the Amplex Red Hydrogen Peroxide/Peroxidase Assay Kit (Invitrogen) while ion leakage was assayed as previously described for barley (Table S1).

2.4 | Effect of methyl viologen-induced ROS on PSII function and disease severity

A fully expanded leaf from the main tiller was dark-adapted for 2 hr, saturated with 0.5 mM methyl viologen (MV; Sigma) to induce ROS and analysed for CF and ion leakage, according to Vicente et al. (2019). To identify differences in disease severity when ROS production was accelerated, plants were sprayed with 100 µM MV and kept in darkness for 30 min before inoculation with *Z. tritici*, after which disease severity was assessed visually, as described above.

2.5 | Extraction and quantification of fungal DNA

Leaf samples were collected from the main tiller at 5 and 14 days postinoculation (dpi), with four replicates for each experimental condition. DNA extraction was as described by Ray et al. (2004). Primers used for quantitative PCR are shown in Table S2. Quantitative PCRs were carried out in a reaction buffer containing 2× SYBR Green Supermix, 250 nM primers, and 20 ng DNA in a final volume of 12.5 µl. Thermal cycling conditions were 3 min at 95 °C; followed by 40 cycles of 10 s at 95 °C, 10 s at 66 °C, and 30 s at 72 °C. Standard curves were obtained from serial dilutions of pure genomic DNA from *Z. tritici* ranging from 1 ng to 10^{-6} ng and were used, with linear regression, to quantify pathogen DNA in samples (pg/ng of total

DNA). Following the final PCR cycle, the specificity of the PCR amplification was checked using a heat dissociation curve from 55 to 95 °C.

2.6 | Gene expression analysis

Leaf samples were collected from whole plants before inoculation and at 8 and 24 hpi for RNA extraction using TRIzol reagent (Invitrogen). RNA was purified with the RNeasy Plant kit (Qiagen) and residual DNA was removed by treating RNA with a RNase-free DNase kit (Qiagen). First-strand cDNA was synthesized using the iScript cDNA synthesis kit (Bio-Rad) according to the manufacturer's protocol. Quantitative reverse transcription PCR (RT-qPCR) was performed in a CFX96 Touch Real-Time PCR Detection System (BioRad,) using a protocol of 30 s at 95 °C, then 40 cycles of 95 °C for 10 s and 60 °C for 15 s. Primers for quantifying target gene expression of wheat and *Z. tritici* and reference genes are shown in Table S2. Gene expression prior to and after inoculation with *Z. tritici* was normalized to the mean C_t values of *CDC*, *ADP*, and *Ubiq* in wheat, whilst *NOXa1* was normalized to the *Z. tritici* elongation factor gene (Table S2).

2.7 | Carotenoid extraction and analysis

Carotenoids were extracted in 100% acetone (HPLC grade), centrifuged at 11,180 × g at 4 °C, and filtered through a 13 mm diameter 0.2 µm polytetrafluoroethylene (PTFE) syringe filter (Whatman). Pigment separation was performed by reverse-phase HPLC as described in Färber et al. (1997). The HPLC analysis was performed using a BioLC HPLC system (Dionex) with LiChrospher 100 RP-18 (5 µm) column (Merck). Three biological replicates, each with three technical replicates, were measured. For each sample the amount of each carotenoid was calculated as a percentage of total carotenoids. In wheat the total carotenoids (Car) comprise neoxanthin, violaxanthin, antheraxanthin, lutein, zeaxanthin, and β-carotene. The size of the xanthophyll cycle (XC) pool of carotenoids, expressed as a percentage of total carotenoids, and de-epoxidation state (DEP) of the xanthophyll cycle pigments were calculated from Equations 1, and 2, respectively.

$$\text{XC pool/Car}(\%) = \frac{\text{Zea} + \text{Anth} + \text{Vio}}{\text{Neo} + \text{Vio} + \text{Anth} + \text{Lut} + \text{Zea} + \beta\text{Car}} \times 100 \quad (1)$$

The DEP of the xanthophyll cycle pigments was calculated using the equation

$$\text{DEP}(\%) = \frac{\text{Zea} + 0.5 \times \text{Anth}}{\text{Zea} + \text{Anth} + \text{Vio}} \times 100 \quad (2)$$

2.8 | Determination of total anthocyanin and phytohormone content

Anthocyanins were extracted from 0.1 g leaf sample with 90% methanol acidified with 0.1% HCl (vol/vol) and quantified by the pH differential method described by Chirinos et al. (2007). Extraction and analyses of phytohormones were as described by Gamir et al. (2012) and Pastor et al. (2018).

2.9 | Leaf gas exchange and CF analysis

CF and gas exchange (GE) were simultaneously measured with an infrared gas analyser (IRGA), LI6400XT, equipped with leaf chamber pulse-amplitude modulated fluorometer LI6400-40 (LI-COR). For all measurements, the IRGA was kept at a gas flow rate of 500 µmol air/s, a cuvette temperature of 22 °C, CO_2 concentration of 400 µl/L, and relative humidity of 60%. CF and GE parameters were measured under actinic light of 1,500 $\mu mol \cdot m^{-2} \cdot s^{-1}$ or in darkness. All measurements were made on the youngest fully expanded leaf on the primary tiller at 24 hpi. Leaves were dark adapted in the growth chamber for 60 min by wrapping sections of the leaf in low-weight aluminium foil. For all measurements, dark-adapted leaves were left for 5 min in the cuvette in darkness until the light period started. Minimal fluorescence (F_o) was measured by applying a low measuring light insufficient to induce significant variable fluorescence, followed by a saturating pulse to determine maximum fluorescence (F_m). Actinic light sufficient to drive photosynthesis was turned on and a saturating pulse of 7,000 $\mu mol \cdot m^{-2} \cdot s^{-1}$ (for 0.8 s) was applied on light-adapted leaves for 2 min to determine maximum fluorescence (F_m'). Actinic light was switched off for 2 s and far-red (FR) light was applied to determine F_o'. Application of a series of saturating pulses every 2 min over a period of 12 min under actinic light and for another 12 min under darkness (actinic light turned off) allowed determination of a series of F_o' and F_m' readings from which time-dependent changes in fluorescence yield were determined. Fluorescence parameters, including nonphotochemical quenching (NPQ), maximum efficiency of PSII photochemistry, PSII maximum efficiency (variable fluorescence/maximum fluorescence, Fv′/Fm′), quantum yield of PSII photochemistry, photochemical quenching (qP), and PSII-driven electron transport rate (ETR) were automatically calculated directly from LICOR 6400XT software using the equations: $(F_m - F_m')/F_m'$, $(F_m - F_o/F_m)$, $(F_m' - F_v')/F_m'$, $(F_m' - F_t)/(F_m')$, $(F_m' - F_t)/(F_m' - F_o')$, and $\{[(F_m' - F_t)/F_m'] \times PPFD \times 0.5 \times a\}$, respectively, where F_t is steady-state fluorescence at a specific time, a is the fraction of incident light that is absorbed by the leaf (assumed to be 0.84) and 0.5 is the approximate fraction of absorbed light directed to PSII in relation to PSI.

Quenching analysis was followed by analysis of relaxation of NPQ kinetics. The rapidly reversible component of NPQ, energy-dependent NPQ (qE), was calculated as $(F_m/F_m') - (F_m/F_m'')$, while the slowly relaxing component (qI) was calculated as $(F_m - F_m'')/F_m''$, where F_m'' is the maximal yield of fluorescence after 12 min of dark relaxation following the actinic illumination. The assumption is that after 12 min of dark treatment, the remaining quenching consists of qI.

Stomatal conductance was also measured in plants kept in darkness from 24 hr before inoculation up to 2 dpi.

2.10 | Statistical analysis

GenStat v. 17.1 (VSN International) was used for all data analysis. In the absence of significant interactions between individual experiments and the main treatments, individual experiments were used as replicates in the analysis. Percentage disease severity was angular transformed to normalize residuals while stomatal conductance was log transformed before analysis. A two-way analysis of variance (ANOVA) with Tukey's multiple comparison test was used except where indicated. Student's *t* tests were used in comparisons between genotypes for anthocyanin concentration, cellular ion leakage, CF, and GE kinetics. Stomatal features were analysed by GenStat unbalanced ANOVA.

3 | RESULTS

3.1 | Characterization of disease phenotypes

Disease symptoms were first visible at 7 dpi on the leaves of Sacramento whereas very few symptoms were observed until 9 dpi on Cougar; by 14 dpi, symptoms were 70% lower on Cougar compared to Sacramento (Figure S1a). Disease development on both genotypes was visually assessed up to 21 dpi (Figure S1b). Areas of chlorotic and necrotic lesions were 90% and 75% less, respectively, in Cougar than in Sacramento at 7 dpi. Necrotic leaf area remained 50% less in Cougar by 16 dpi (Figure S1c–e). There were no differences between genotypes in the amount of pathogen DNA at 5 dpi but at 14 dpi pathogen DNA was significantly lower in Cougar compared to Sacramento (Figure S1f).

3.2 | qI form of NPQ and increased stomatal responsiveness in darkness contribute to the disease response in the resistant genotype

NPQ induction and relaxation kinetics were measured during transition from dark-adaptation to 1,500 $\mu mol \cdot m^{-2} \cdot s^{-1}$ light at 24 hpi. Under high light, NPQ was significantly higher in Cougar compared to Sacramento irrespective of inoculation (Figure 1a,f), with relaxation of quenching inhibited in darkness once infected (Figure 1f). The majority of NPQ in both genotypes was of qE form (Figure 2a); however, a significantly higher proportion of qI (33%) remained in Cougar after infection (Figure 2b). *Z. tritici* infection caused a significant decrease in maximum quantum yield of photosystem (PSII) (F_v/F_m) in leaves of Cougar following 60 min of dark adaptation, but this was not observed in Sacramento (Figure 2c). After 12 hr in darkness, F_v/F_m in Cougar infected with *Z. tritici* recovered to the same level as the water-treated plants (data not shown).

After mock inoculation, electron transport rate (ETR), photochemical quenching (qP), photosynthesis, and stomatal conductance were less in Cougar compared to Sacramento (Figure 1b–e). However, after infection, no differences were observed between genotypes (Figure 1g–i), except for rapid stomatal closure in darkness in the resistant genotype (Figure 1j).

3.3 | Light drives ROS-accumulation in the host and ROS-encoding gene expression in the pathogen

Histochemical staining with DAB showed strong brown staining in the leaves of Sacramento at 8 hpi but decreased gradually from 24 hr to 2 dpi before reaching another peak at 12 dpi (Figure 3a). The trend was similar in Cougar, although leaf tissues stained more faintly. Significantly higher accumulation of H_2O_2 coupled with higher ion leakage was observed in Sacramento compared to Cougar (Figure 3b,d). Lower H_2O_2 concentrations were quantified in the dark-adapted *Z. tritici*-infected plants, although a transient increase in H_2O_2 was briefly induced in Cougar at 8 hpi (Figure 3b). The most common ROS originating in the chloroplast (from PSII) is $O_2^{\bullet -}$. On staining with NBT, with added sodium azide to inhibit reduction by oxidoreductases in the plant, Sacramento leaves stained dark blue from 4 hpi until 2 dpi while no staining was observed in Cougar (Figure 3c) suggesting absence of $O_2^{\bullet -}$. We also quantified the gene expression of the NADPH-dependent oxidase activator 1 (*NOXa1*), which modulates superoxide production in *Z. tritici* (Choi et al., 2016). *NOXa1* was up-regulated in the interaction with the susceptible genotype of Sacramento compared to the resistant Cougar (Figure 3e), whereas in sustained darkness, *NOXa1* was down-regulated in both genotypes by 24 hpi (Figure 3e), indicating *Z. tritici* required light for *NOXa1* expression.

3.4 | Chloroplast-specific antioxidant systems are induced under light conditions in the resistant Cougar

The resistant genotype accumulated less H_2O_2 and no visible $O_2^{\bullet -}$ during interaction with the pathogen under light conditions, and these findings together with the up-regulation of qI suggested enhanced ability to detoxify ROS, probably via the action of xanthophylls and through enhanced activity of antioxidant enzymatic systems. Expression of iron dismutase (*FeSOD*), an enzyme present exclusively in the chloroplast (Alscher et al., 2002), and glutathione peroxidase (*GPX*) was three-fold higher in Cougar compared to Sacramento at 24 hpi (Figure S2a,b). Copper-zinc superoxide dismutase (*Cu/ZnSOD*) was down-regulated in Cougar after infection but remained highly expressed in Sacramento (Figure S2c). Manganese superoxide dismutase (*MnSOD*), catalase (*CAT*), and peroxisomal ascorbate peroxidase (*APX*) were strongly induced in Sacramento but not in Cougar (Figure S2d–f).

To determine whether light influenced the expression of genes encoding antioxidant enzymes in infected plants, we measured their relative expression in plants kept in darkness for up to 24 hpi. All genes were down-regulated in both genotypes at 8 hpi, but by 24 hpi, *Cu/ZnSOD*, *MnSOD*, and *APX* were up-regulated in Sacramento whilst *CAT* was up-regulated in Cougar (Figure S2g–l).

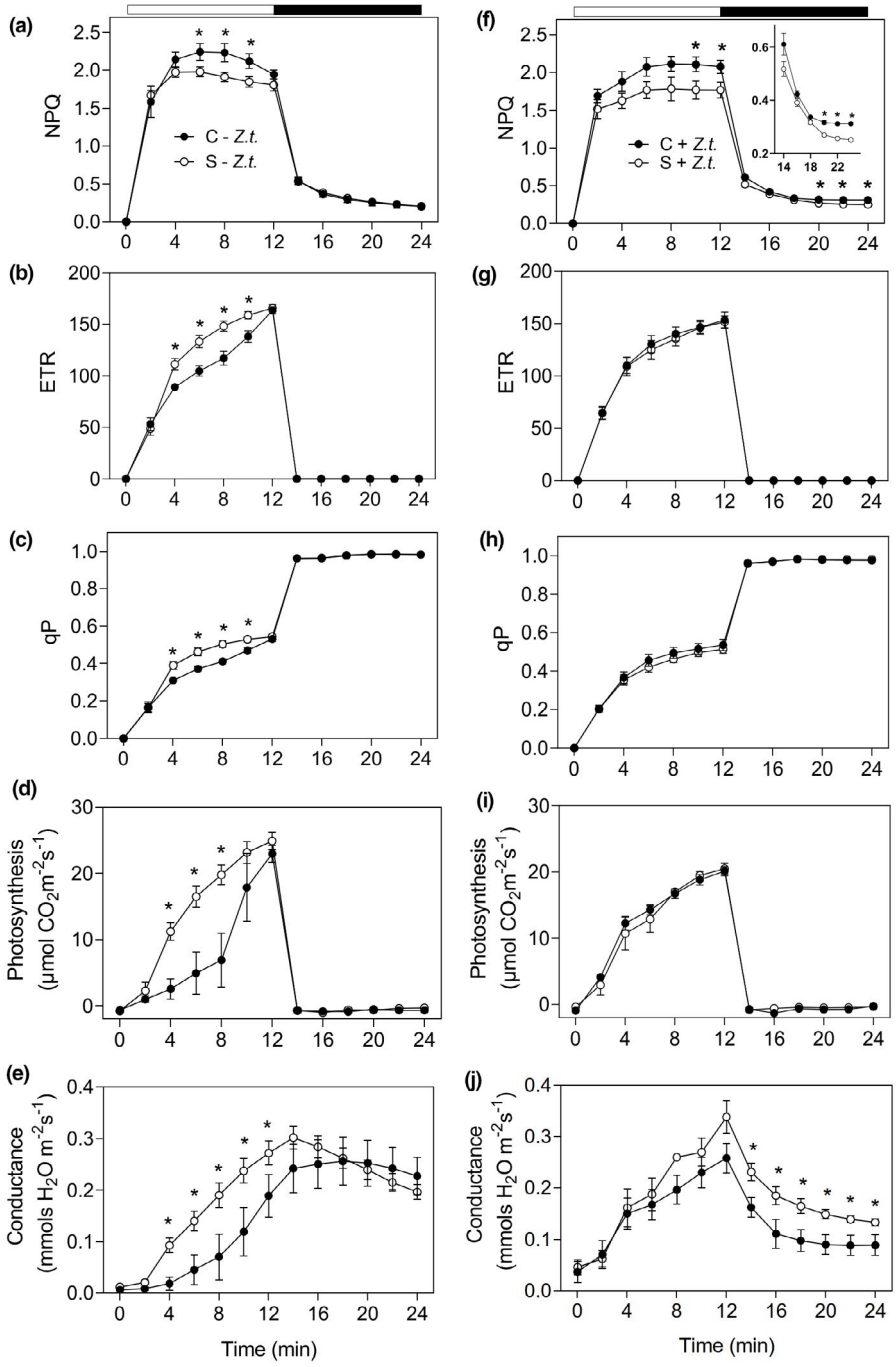

FIGURE 1 Chlorophyll fluorescence and gas exchange kinetics in wheat genotypes Cougar and Sacramento up to 24 hr postinoculation (hpi) with *Zymoseptoriatritici*. (a,f) Nonphotochemical quenching (NPQ), (b,g) electron transport rate (ETR), (c,h) photochemical quenching (qP), (d,i) rate of photosynthesis, (e,j) stomatal conductance. Dark-adapted leaves were illuminated with a light intensity of 1,500 µmol·m^{-2}·s^{-1} (white bar) for the first 12 hpi followed by dark relaxation kinetics in darkness (black bar). Inoculated plants were sprayed with a *Z. tritici* isolate (10^6 spores/ml). Measurements were made on the youngest fully expanded leaves on the primary tiller. +*Z.t.*, *Z. tritici* inoculated; −*Z.t.*, water-treated control. C, Cougar; S, Sacramento. Data represent mean ± *SEM* of eight biological replicates. An asterisk indicates a significant difference according to Student's *t* test, $p < 0.05$

We assessed the tolerance of the two genotypes to excessive accumulation of $O_2^{\bullet-}$ by methyl viologen (MV) treatment as loss of photosynthetic performance. There was no difference in F_v/F_m between MV-treated and water-treated plants (Figure S3a). NPQ increased but ETR and qP decreased due to MV, suggesting electron transport between PSII and PSI was inhibited in both genotypes (Figure S3b–d). Comparison between MV-treated Cougar and Sacramento showed higher ETR and qP and less cellular leakage in Cougar (Figure S3c–e), suggesting more efficient superoxide detoxification. Furthermore, MV treatment resulted in more rapid and severe disease development in Cougar 7 dpi, implying increased susceptibility to *Z. tritici* from over-accumulation of $O_2^{\bullet-}$ (Figure S3f).

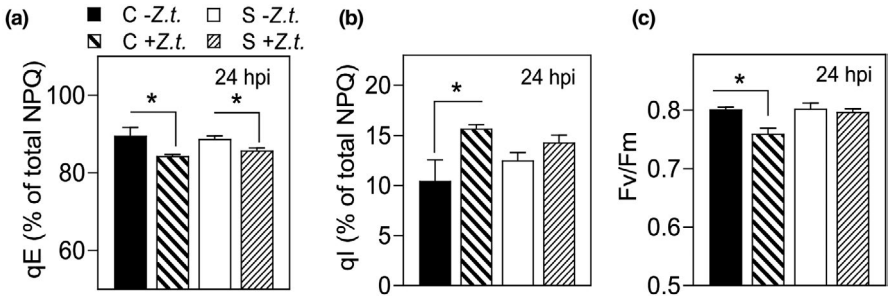

FIGURE 2 Nonphotochemical quenching (NPQ) components qE and qI expressed as percentage values and maximum photochemical efficiency of photosystem II (variable fluorescence/maximum fluorescence, F_v/F_m) in leaves of wheat genotypes Cougar and Sacramento up to 24 hr postinoculation (hpi). qE: Energy quenching, qI: photoinhibitory quenching. +*Z.t.*, *Zymoseptoria tritici* inoculated; –*Z.t.*, water-treated control; C, Cougar; S, Sacramento. Data represent mean ± *SEM* of eight biological replicates. An asterisk indicates a significant difference according to Student's *t* test, $p < 0.05$

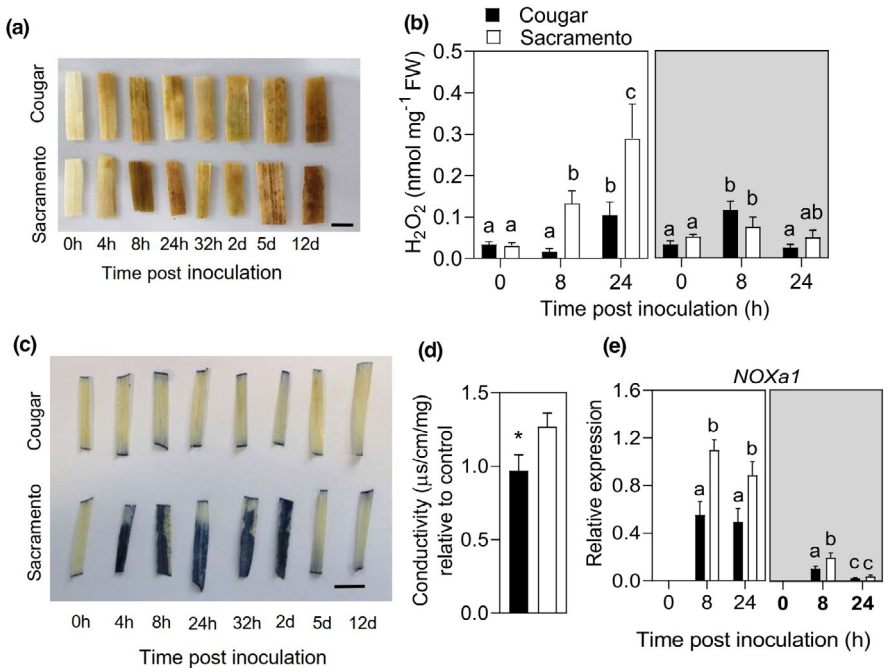

FIGURE 3 Concentration of reactive oxygen species (ROS) and tissue cellular leakage in leaves of wheat genotypes Cougar and Sacramento in response to infection by *Zymoseptoriatritici*. (a) Hydrogen peroxide (H_2O_2) accumulation was visualized by 3,3′-diaminobenzidine (DAB) staining. Scale bar = 1 cm. (b) H_2O_2 content was quantified before and after inoculation in light- (unshaded box) and dark-adapted (shaded box) leaves of Cougar and Sacramento. (c) Superoxide accumulation visualized by nitroblue tetrazolium (NBT) staining with added sodium azide. Bar = 1 cm. (d) Leaf cellular leakage from light-adapted leaves 24 hr postinoculation (hpi) of four biological replicates. Asterisk indicates a significant difference according to Student's *t* test, $p < 0.05$. (e) Expression of *Z. tritici* gene encoding NADPH oxidase activator 1 (*NOXa1*) in light- and dark-adapted leaves of Cougar and Sacramento. Data represent means ± *SEM* of six biological replicates. Different letters above the bars indicated significant differences according to analysis of variance followed by Tukey's test ($p < 0.05$)

3.5 | Photoprotection in the resistant genotype is associated with high carotenoid:chlorophyll (Car:Chl) and biosynthesis of neoxanthin and ABA

To determine the effect of *Z. tritici* on the biosynthesis of xanthophylls, we quantified pigment composition and measured differential gene expression in the pathway before inoculation and at 8 and 24 hpi (Table 1, Figure 4). There was no difference between genotypes in Chl *a*:*b* before inoculation, and Cougar intrinsically possessed higher Car:Chl, lutein, and lower xanthophyll pool (XC) size compared to Sacramento (Table 1). At 8 hpi, Chl *a*:*b*, lutein (Table 1), and β-carotene decreased in Cougar, the latter consistent with down-regulation of *BCH* regulating the XC pool size (Davison et al., 2002) and thus affecting the Car:Chl (Figure 4). Car:Chl increased in both genotypes whilst the XC pool decreased in Sacramento (Table 1). By 24 hpi, the XC pool continued to decrease in Sacramento accompanied by an DEP, whilst Chl *a*:*b*, lutein, DEP, and the XC pool (Table 1) recovered in Cougar with the slight but significant increase of antheraxanthin

Pigment	0 hpi		8 hpi		24 hpi	
	Cougar	Sacramento	Cougar	Sacramento	Cougar	Sacramento
Chl *a*:*b*	2.13 a	2.30 a	1.26 b	2.00 a	1.64 c	2.19 a
Car:Chl	0.61 a	0.51 b	1.45 c	0.56 a	1.11 d	0.68 a
Lutein	62.12 a	60.76 b	56.32 c	60.83 b	58.35 d	61.44 ab
XC pool	18.33 a	21.20 b	18.45 a	19.99 c	19.41 c	17.29 ac
DEP	13.97 a	10.58 b	9.79 c	16.87 d	18.17 e	31.75 f

TABLE 1 Pigment content of leaves of wheat varieties Cougar and Sacramento before and after inoculation with *Zymoseptoria tritici*

Note: Chl, chlorophylls; Car:Chl, ratio of total carotenoids to chlorophylls; XC, xanthophyll cycle; DEP, de-epoxidation state; hpi, hours postinoculation.

Across rows, different letters after values indicate a significant difference according to analysis of variance followed by Tukey's test ($p < 0.05$).

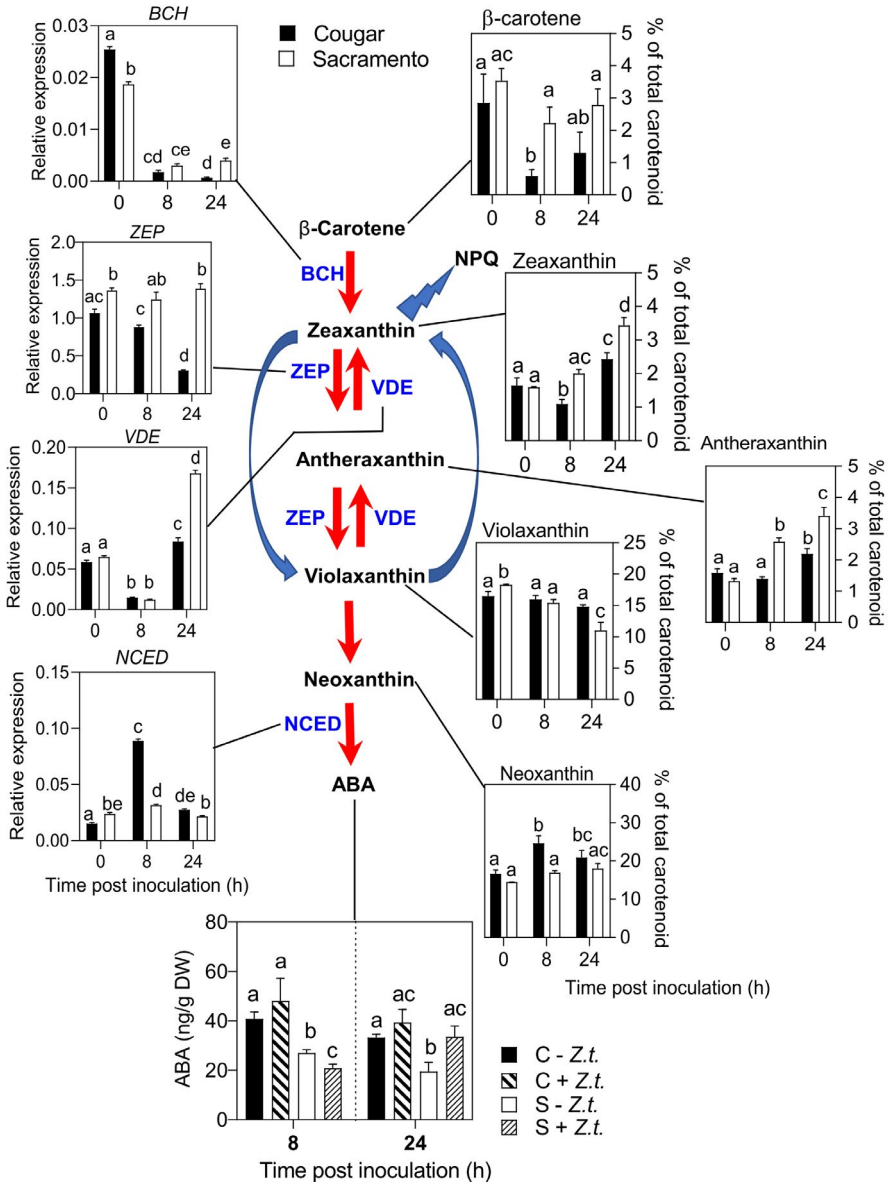

FIGURE 4 Effect of *Zymoseptoriatritici* on β-carotene-derived xanthophylls and abscisic acid (ABA) biosynthesis in wheat genotypes Cougar and Sacramento. Schematic representation of biosynthetic pathway of β-carotene-derived xanthophylls highlighting time courses of changes in gene expression, xanthophylls and ABA contents. *BCH*, β-carotene hydroxylase; *VDE*, violaxanthin de-epoxidase; *ZEP*, zeaxanthin epoxidase; *NCED*, 9-*cis*-epoxycarotenoid dioxygenase; NPQ, nonphotochemical quenching. Data represent means ± *SEM* of six biological replicates. Different letters above the bars indicate significant differences according to analysis of varaince followed by Tukey's test ($p < 0.05$)

and zeaxanthin (Figure 4). Notably, at 24 hpi, Cougar remained with significantly higher Car:Chl, lower Chl *a*:*b*, and lower DEP compared to Sacramento (Table 1). *ZEP* expression remained significantly lower in Cougar and decreased at 24 hpi (Figure 4). VDE was down-regulated in both genotypes at 8 hpi and recovered by 24 hpi, remaining highly expressed in Sacramento. These changes in gene expression were consistent with the observed decrease in DEP and zeaxanthin in Cougar and the increase in DEP, antheraxanthin, and zeaxanthin in

Sacramento (Figure 4). Zeaxanthin is epoxidized by *ZEP* to produce violaxanthin from which neoxanthin is synthesized and we observed an increase in neoxanthin in Cougar in contrast to an increase in zeaxanthin in Sacramento (Figure 4). Cleavage of neoxanthin by the enzyme 9-*cis*-epoxy-carotenoid dioxygenase (NCED) represents the first committed step in ABA biosynthesis (Chernys & Zeevaart, 2000). *NCED* expression was induced in both genotypes at 8 hpi; however, quantified endogenous ABA was significantly higher in Cougar compared to Sacramento, with the latter showing ABA decline due to inoculation (Figure 4). At 24 hpi, there was still no significant effect of infection on ABA in Cougar whilst ABA recovered in Sacramento (Figure 4).

3.6 | Differential leaf traits and pathogen behaviour

ABA is a major regulator of stomatal development, morphology, and function and modulates the formation of cuticular wax on leaf surfaces, which can influence fungal infection by foliar pathogens (Ziv et al., 2018). Examination of the adaxial leaf surfaces of the genotypes (Figure 5a,b) showed narrow and significantly longer stomata with reduced density in Cougar compared to Sacramento (Figure 5c–e). Prior to inoculation, the fatty acyl-CoA reductase (*TaFAR3*) encoding the biosynthesis of cuticle wax on leaf tissues was more highly expressed ($p < 0.05$) in Cougar compared to Sacramento. Infection with *Z. tritici* reduced *TaFAR3* expression in Cougar in contrast to Sacramento (Figure S4).

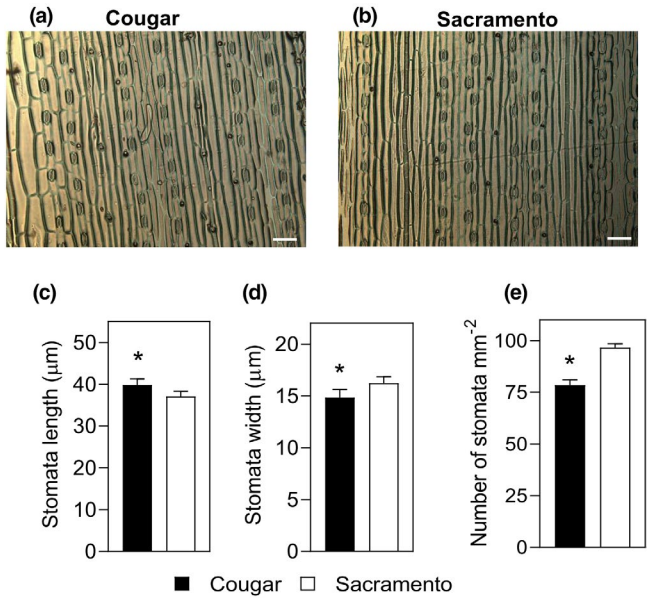

FIGURE 5 Stomatal characteristics in noninoculated wheat genotypes Cougar and Sacramento. Comparison of adaxial epidermal imprint obtained from images of Cougar (a) and Sacramento (b); bar = 50 µm. (c) Stomatal length, (d) stomatal width, and (e) number of stomata (per mm^2). Data represent means ± *SEM* of four biological replicates. An asterisk indicates a significant difference according to Student's *t* test, $p < 0.05$

To identify differences in behaviour of *Z. tritici* on the leaf surface of the genotypes, we carried out microscopic examinations at 2, 5, and 21 dpi (Figure 6a–f). At 2 dpi, on Cougar leaves, *Z. tritici* extended germ tubes from the two terminal points of the germinated spore, resulting in significantly longer and unbranched hyphae lacking consistent directional growth towards stomata (Figure 6a,g,h). On Sacramento, shorter hyphae originating from multiple terminal points were excessively branching to reach the stomata in closest proximity (Figure 6d,g,h). By 5 dpi, pathogen growth was slow and lacked mycelial mass on Cougar while compact mycelial networks were formed in Sacramento (Figure 6b,e). At 21 dpi, abundant pycnidia in substomatal cavities were evident in Sacramento whilst, in Cougar, short mycelia were seen extruding from stomatal cavities (Figure 6c,f). To determine if the behaviour of the pathogen on the leaf surfaces was due to differences in initial germination rates, we analysed spore germination and germ tube extension in vitro. Compared to the control, *Z. tritici* on Sacramento leaves showed increased germination at 2 hpi followed by extension of longer germ tubes at 8 hpi, whereas no differences were observed between Cougar and the control (Figure 6i,j).

3.7 | Stomatal function and photosynthetic cost of *Z. tritici* infection

To determine the comparative photosynthetic cost of resistance or susceptibility to *Z. tritici*, we measured GE and CF in both Cougar and Sacramento at 8 hpi, 24 hpi, 2 dpi, and at 5 dpi. Stomata of most plants typically open in response to light stimulus and high humidity and close in darkness. *Z. tritici* increased stomatal conductance in both genotypes in light and darkness until 2 dpi (Figure 7a,b). We also observed an increased rate of leaf transpiration in the infected plants of both genotypes compared to the water-treated controls at 8 hpi and 2 dpi, and intercellular CO_2 at 24 hpi and at 2 dpi (Table S3). These results suggest that *Z. tritici* was able to manipulate stomatal function at early stages of disease progression and this process was independent of resistance.

Z. tritici infection led to a significant decrease in F_v/F_m in Cougar at 8 hpi, 24 hpi, and 2 dpi but recovered at 5 dpi whilst no significant differences were observed for Sacramento (Figure S5a). NPQ decreased in both genotypes but not at 24 hpi for Cougar (Figure S5b). In contrast to Sacramento, PSII maximum efficiency (F_v'/F_m') decreased significantly in inoculated plants of Cougar compared to the control at 24 hpi. F_v'/F_m' remained higher in Sacramento compared to Cougar irrespective of infection for the rest of the time measurements (Table S4). Cougar was characterized by higher qP than Sacramento but *Z. tritici* down-regulated ϕPSII and qP at 5 dpi in both genotypes (Table S4). Photosynthesis decreased by 27% in Cougar at 24 hpi followed by a 40% increase by 2 dpi (Figure 7c). In Sacramento, the effect of infection was detected at 5 dpi with 58% decrease in net photosynthesis accompanied by reduced stomatal conductance (Figure 7a,c), suggesting impaired stomatal function at this stage of infection. At the same time, photosynthesis and

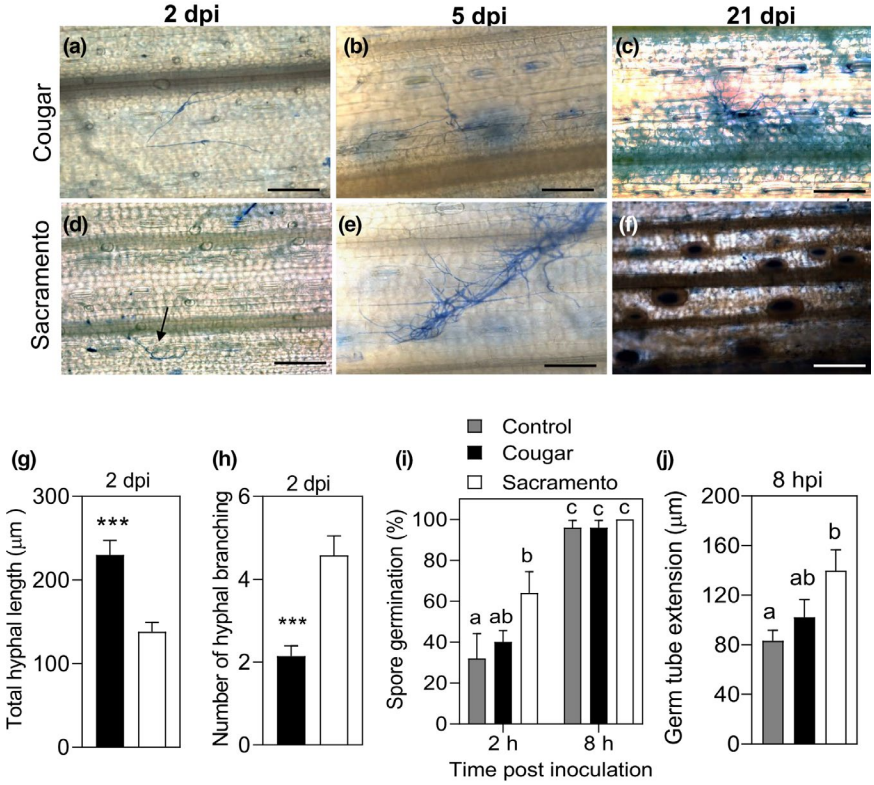

FIGURE 6 Growth of *Zymoseptoriatritici* on leaf surfaces of wheat genotypes Cougar and Sacramento and in in vitro assays. Hyphal growth habit on leaf surface of Cougar (a–c) and Sacramento (d–f) at 2, 5, and 21 days postinoculation (dpi). In Sacramento aggregation of hyphal clusters in substomatal cavities at 5 dpi (e), pycnidia formation at 21 dpi (f) can be seen; bar = 500 µm. (g) Total hyphal length and (h) hyphal branch length of *Z. tritici* per mm^2 leaf area surface at 2 dpi. (i) Percentage germination rate of *Z. tritici* spores and (j) germ tube extension from germinating Z. *tritici* spores on Cougar and Sacramento in comparison to the control samples lacking plant tissue. Data represent means ± *SEM* of five biological replicates. Different letters above the bars indicate significant differences ($p < 0.05$) according to analysis of variance followed by Tukey's test. Triple asterisks indicates a significant difference according to Student's *t* test, $p < 0.001$

stomatal conductance remained higher in Cougar than in Sacramento (Figure 7a,c).

3.8 | JA, in antagonistic action to SA, is associated with defence against *Z. tritici* in the resistant cultivar Cougar

ABA has been shown to promote either resistance or susceptibility depending on the timing of interaction with other signalling phytohormones (Ton et al., 2009). To determine whether different levels of endogenous ABA in our genotypes were associated with differences in SA-dependent defence responses, we measured the relative expression of SA-dependent pathogenesis-related (PR) genes, *PR1* and *PR5* (thaumatin/osmotin-like protein). *Z. tritici* induced expression of *PR1* and *PR5* at 8 hpi in Sacramento whereas small increases were observed in Cougar at 24 hpi (Figure S6a,d), implying stronger activation of the SA signalling pathway in Sacramento. Expression of *PAL* and *ICS*, encoding phenylalanine ammonia-lyase and isochorismate synthase enzymes, respectively, required for the biosynthesis of SA in plants, showed greater basal levels in Cougar compared to Sacramento (Figure 8a,b). However, in Sacramento, *PAL* was induced from 8 hpi and both genes were strongly induced at 24 hpi. In Cougar, *ICS* was down-regulated at 8 hpi and both genes were slightly up-regulated at 24 hpi. (Figure 8a,b). Analysis of endogenous SA concentration showed greater accumulation of SA in Sacramento compared to Cougar at 8 hpi, irrespective of inoculation (Figure 8c). At 24 hpi, SA decreased by 21% in Cougar compared to control plants (Figure 8c). The PAL pathway in plants contributes to the biosynthesis of secondary antimicrobial metabolites involved in defence fortification including lignin (Zhang & Liu, 2015). Staining with toluidine blue O showed lignification of leaves of Cougar at 0 and 8 hpi, and in Sacramento at 24 hpi (Figure S7).

SA and JA defence pathways are known to be mutually antagonistic in action (Li et al., 2019). Therefore, we examined the expression of *PR2* (β-1,3-glucanase) and *PR3* (chitinase), both JA signalling markers previously shown to have antifungal activity against *Z. tritici* in wheat (Shetty et al., 2009). *PR2* and *PR3* were strongly induced at 8 hpi in Cougar and down-regulated significantly in both genotypes by 24 hpi (Figure S6b,c).

The contrasting expression of phytohormone markers together with quantification of ABA and SA in our genotypes suggested that JA is probably biosynthesized in Cougar to contribute

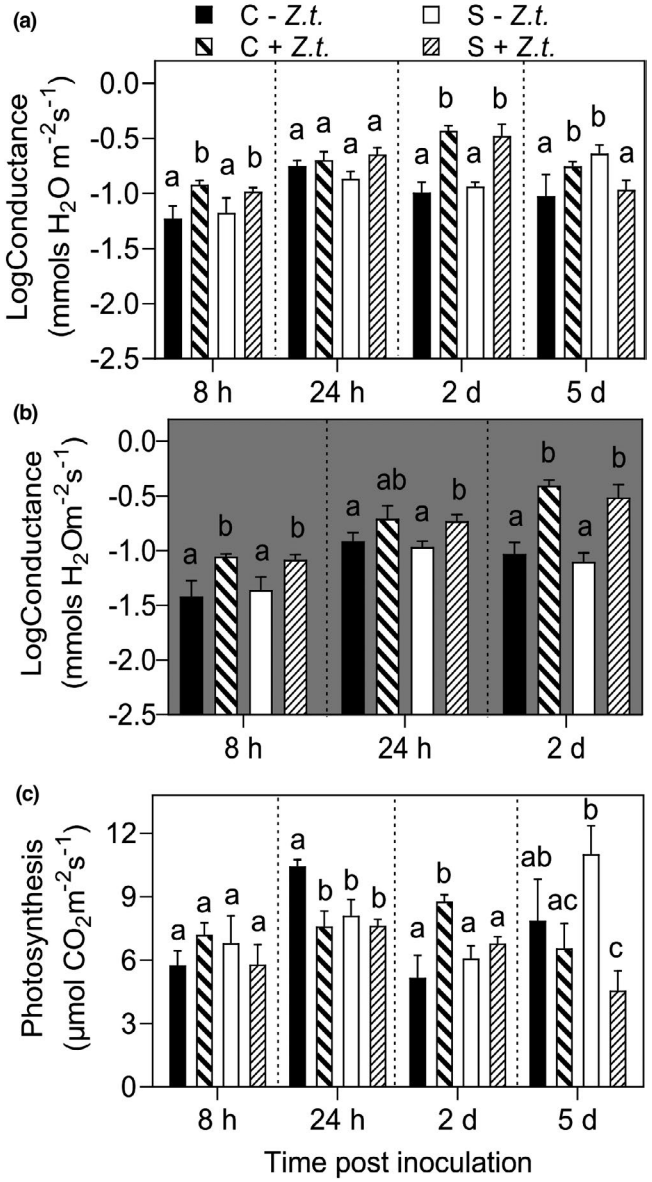

FIGURE 7 Effect of *Zymoseptoriatritici* on gas exchange in wheat genotypes Cougar and Sacramento at 8 hr postinoculation (hpi), 24 hpi, 2 days postinoculation (dpi) and 5 dpi. (a,b) Stomatal conductance (log transformed) in plants under (a) light conditions and (b) dark-adapted state. (c) Rate of leaf photosynthesis. Actinic light was 1,500 µmol·m^{-2}·s^{-1}. Data represent means ± *SEM* of eight biological replicates. Different letters above the bars indicate significant differences ($p < 0.05$) according to analysis of variance followed by Tukey's test. +Z.t., *Z. tritici* inoculated; −Z.t., water-treated control; C, Cougar; S, Sacramento

to ABA/JA-driven defence. First, we quantified the expression of genes encoding enzymes in the JA biosynthetic pathway including lipoxygenase (*LOX*), allene oxide synthase (*AOS*), and allene oxide cyclase (*AOC*) (Figure 8d–f) and endogenous concentrations of 12-oxo-phytodienoic acid (OPDA), a JA precursor, and free JA in water-treated controls and *Z. tritici*-inoculated leaves of Cougar and Sacramento at 8 and 24 hpi (Figure 8g,h). The expression trends over time for *LOX*, *AOS*, and *AOC* were similar, showing greater expression in Cougar compared to Sacramento prior to inoculation. These genes became induced by *Z. tritici* at 8 hpi in both genotypes but significantly more in Cougar than in Sacramento. By 24 hpi all genes were down-regulated in both genotypes (Figure 8d–f). OPDA significantly decreased in both genotypes in response to infection but remained significantly higher in Cougar than in Sacramento (Figure 8g). JA concentration in Cougar was 75% higher than Sacramento irrespective of infection (Figure 8h) and by 24 hpi remained only in Cougar while we were unable to detect it in Sacramento (Figure 8h). We also assessed concentration of anthocyanins in both genotypes as they are known JA-stimulated secondary metabolites synthesized via PAL and crucial in plant defence against fungal pathogens. Concentrations were similar in both genotypes before inoculation; however, a biphasic accumulation of anthocyanin was observed in Cougar, with early and late peak profiles at 8 hpi and 2 dpi, respectively. In contrast, anthocyanins decreased in Sacramento from 4 hpi until 32 hpi, followed by a rapid rise, similar to that in Cougar, from 2 dpi (Figure 8i).

4 | DISCUSSION

Despite the importance of the chloroplast as a major site of photosynthesis and production of key defence molecules, there have been few studies on understanding the mechanistic link between photoprotection and plant defence against fungal pathogens. Here, we have shown two contrasting photoprotection responses of wheat genotypes but only one of them was associated with enhanced defence against *Z. tritici*. Successful defence in Cougar, in contrast to Sacramento, was characterized by effective energy regulation via qE and qI types of NPQ by the XC, and optimization of light harvesting by redistribution of chlorophyll in the light harvesting complexes of PSII resulting in an increased ratio of total carotenoids to chlorophylls. Of the three major carotenoid xanthophylls in leaves (lutein, violaxanthin, and neoxanthin), lutein is the predominant xanthophyll in plants and is evolutionarily conserved, accounting for c.60% of the carotenoids in leaves of wheat genotypes in this study. In response to *Z. tritici*, lutein decreased significantly in Cougar allowing for compensatory increase in the biosynthesis of neoxanthin at 8 hpi. We also measured higher endogenous ABA in Cougar than in Sacramento. ABA regulates stomatal patterning and development in plants (Chater et al., 2014), and in our studies, quantified ABA supported the observed differences in stomatal anatomical features and stomatal operational control of the genotypes. Cougar possessed long, sparse stomata with narrow apertures in contrast to Sacramento, where the pathogen benefitted from the presence of dense stomata with wider aperture. In vitro assays and microscopic observations revealed that *Z. tritici* germinated rapidly, within 2 hr of exposure to the susceptible host, Sacramento, and extended short, numerous hyphal branches. Cougar appeared less hospitable to the pathogen, as shown by the low rate of spore germination (similar to the water control) and the lack of hyphal branching on the leaf. Furthermore, at 8 hpi, *PR2* and *PR3*, which act synergistically on

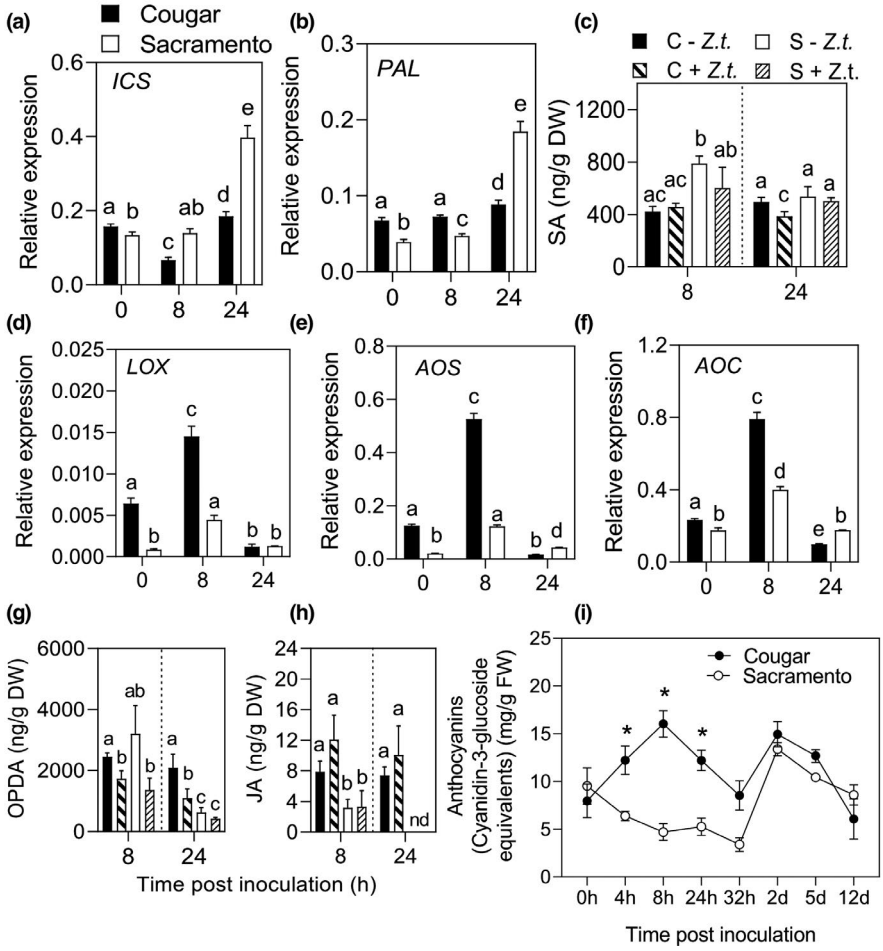

FIGURE 8 Effect of *Zymoseptoriatritici* on the expression of phytohormone biosynthetic genes, phytohormone content, and total anthocyanin content in leaves of wheat genotypes Cougar and Sacramento. Expression of (a) isochorismate synthase (*ICS*), (b) phenylalanine ammonia-lyase (*PAL*), (d) lipoxygenase (*LOX*), (e) allene oxide synthase (*AOS*), and (f) allene oxide cyclase (*AOC*) before inoculation, and at 8 and 24 hr postinoculation (hpi) by quantitative reverse transcription PCR. Data represent means ± *SEM* of six biological replicates. Concentrations of (c) salicylic acid (SA) (g) *cis*-(+)-12-oxo-phytodienoic acid (OPDA) and (h) jasmonic acid (JA) in leaves of water-treated control (–*Z.t.*) and *Z. tritici*-inoculated (+*Z.t.*) plants at 8 and 24 hpi. (i) Total anthocyanin content expressed as cyanidin-3-glucoside equivalents in mg/L at different time points after infection by *Z. tritici*. Data represent means ± *SEM* of four biological replicates. Phytohormone concentrations were expressed as dry weight (DW). Different letters above the bars indicate significant differences according to analysis of variance followed by Tukey's test ($p < 0.05$). Statistical differences between genotypes for total anthocyanin content at each time point were analysed by Student's *t* test. $^*p < 0.05$. nd, not detected; C, Cougar; S, Sacramento

fungal cell wall hydrolysis to inhibit hyphal growth in vivo and in vitro in fungi, were up-regulated in Cougar in contrast to Sacramento. The extension of long, apical-end hyphae, as seen in Cougar, are likely to consume more energy in time and have been shown in other experiments to be typical fungal behaviour in nutritionally poor environments, including water (Walker & White, 2017). Random hyphal growth on Cougar leaves also suggested that stomata were not as easily located as in Sacramento. Increased leaf cuticular waxing has been suggested to play a role in masking stomata from pathogen hyphae of rusts (Rubiales & Niks, 1996). We did not measure wax deposition in this work, but we measured the expression of *TaFAR3*, which catalyses the production of C28 alcohol, a major cuticular wax component found in wheat leaves, particularly at seedling stage (Wang et al., 2016). *TaFAR3* was constitutively expressed in Cougar before infection but was down-regulated after infection in a time-responsive manner. A strong link between cuticle formation and epidermal patterning exists, with the former also modulated by ABA (Chater et al., 2014). Plants with larger stomata at reduced density also have reduced responsiveness to increasing light intensity and conductance compared to plants with shorter and dense stomata (Faralli et al., 2019). Indeed, in the absence of infection, Cougar exhibited slower stomatal kinetics to light stimulus compared to Sacramento. However, in the presence of *Z. tritici* at 24 hpi in darkness, we observed increased stomatal responsiveness of Cougar compared to Sacramento, coinciding with ABA accumulation causing stomatal closure, thus reducing stomatal conductance. This potential advantage of Cougar may act to delay but not prevent pathogen entry, as our additional measurements of stomatal conductance showed that up to 2 dpi, *Z. tritici* effectively hijacked stomatal control by enhancing stomatal sensitivity to light and

increasing conductance, irrespective of differences in resistance in our genotypes or the external stimulus. Stomata in infected plants also appeared unresponsive to high intercellular CO_2 concentration after inoculation, in addition to increased transpiration, thus creating conditions favourable for hyphal growth. These results suggested that *Z. tritici* benefited from light during the early infection process. Further evidence that light enhanced pathogenesis was provided by the significant up-regulation in *Z. tritici* of *NOXa1*, encoding NADPH oxidase, which transfers electrons from NAPDH to oxygen molecules, at 8 and 24 hpi in Sacramento compared to in Cougar, coinciding with the increased abundance of $O_2^{\bullet-}$ and H_2O_2 in the former. In contrast, in darkness, fungal gene expression diminished and lower concentrations of H_2O_2 were measured in both genotypes. Choi et al. (2016) showed that the expression of *NOXa1* resulting in ROS formation ($O_2^{\bullet-}$) was an important determinant for virulence and pathogenicity of *Z. tritici* in wheat. These findings imply that the pathogen exploits light to both hijack stomatal control and increase oxidative stress in the host by additional $O_2^{\bullet-}$ formation, which over time will render PSII more vulnerable to light-induced photodamage and so hasten host cell death (Govrin & Levine, 2000). Indeed, in Sacramento, increase in ROS accompanied by down-regulation of chloroplast-specific scavengers for $O_2^{\bullet-}$ resulted in increased disease progression and tissue damage, consistent with our observations of higher cellular ion leakage and greater disease severity. We showed that Cougar was more tolerant to $O_2^{\bullet-}$ induced by MV and was able to maintain higher ETR and qP compared to Sacramento as well as exhibiting lower cellular ion leakage following MV treatment. However, excessive $O_2^{\bullet-}$ due to the herbicide still resulted in enhanced susceptibility of the resistant genotype to *Z. tritici* suggesting that oxidative stress due to $O_2^{\bullet-}$ can compromise plant immunity of this genotype. In darkness, there was a 4-fold decrease in H_2O_2, which, in the absence of differential expression of genes encoding detoxification molecules, suggested that production by both the host and the pathogen ceased.

Plants use ROS as molecular messengers in signalling and activation of HR during the defence response by simultaneously forming ROS whilst down-regulating ROS-scavenging and detoxification (Apel & Hirt, 2004). Thus, cellular oxidative homeostasis is tightly managed by the activities of APX, CAT, and SODs suppressing $O_2^{\bullet-}$, H_2O_2, and OH. Similar to previous studies by Shetty et al. (2003), under light conditions we observed an inverse relationship between H_2O_2 abundance and gene expression of antioxidants such as *APX*, *CAT*, *MnSOD*, and *Cu/ZnSOD* in the resistant genotype but not in the susceptible genotype. In parallel, the chloroplast-specific antioxidant gene encoding *FeSOD*, known to target $O_2^{\bullet-}$ generated in the chloroplast, was induced in Cougar whilst the opposite was observed in Sacramento, where *APX*, *CAT*, *MnSOD*, and *Cu/ZnSOD* were up-regulated. These results, together with the absence of $O_2^{\bullet-}$ in Cougar, suggest that chloroplast-specific antioxidants in the resistant genotype acted to regulate $O_2^{\bullet-}$. In contrast, in Sacramento, ROS as $O_2^{\bullet-}$ formed at PSI side in the chloroplast, and was most probably converted to H_2O_2 by SODs and further reduced to H_2O by GPX and CAT.

A small amount of ROS is required to trigger production of redox signals that in turn induce the synthesis of factors necessary for NPQ and lipid peroxidation via LOX for JA biosynthesis, and also triggers de novo synthesis of compounds such as carotenoids (Demmig-Adams et al., 2013). This is achieved by down-regulation of NPQ acting as a positive regulator of PAMP-triggered immunity (PTI; Göhre et al., 2012) with significant impact on the plant photosynthetic response (de Torres Zabala et al., 2015). Lee et al. (2015) showed that the PTI response in wheat leaves requires both chitin elicitor receptor kinase 1 (CERK1) and chitin elicitor binding protein (CEBiP) for perception of chitin of *Z. tritici* during early infection. *Z. tritici* encodes Mg3LysM protein, which acts to suppress chitin-initiated defence, whilst Mg1LysM and Mg3LysM also bind chitin and thus avoid detection by the host receptors (Kettles & Kanyuka, 2016). In these studies, we showed that *PR2* (glucanase) and *PR3* (chitinase) were up-regulated at 8 hpi in Cougar, suggesting that the initial PTI response may have been induced in this genotype. However, further experiments are necessary to show whether PTI was indeed more effective in Cougar than in Sacramento.

Down-regulation of photosynthetic efficiency upon infection allows plants to mount early defence signalling and to divert the major flow of assimilates from primary metabolism to synthesize secondary metabolites such as flavonoids and anthocyanins. Anthocyanins, derived from the phenylpropanoid pathway in a trade-off to photosynthesis, function photoprotectively in plants via their significant ability to modify both the quantity and quality of light incident on chloroplasts and by ROS scavenging (Steyn et al., 2002). PAL is an upstream enzyme in the phenylpropanoid pathway and its up-regulation is often used as a marker for the biosynthesis of many secondary metabolites that are important in plant defence including, in addition to anthocyanins, lignin and SA (Huang et al., 2010). However, SA is also biosynthesized via the ICS pathway in plants and its pathogen-induced accumulation plays a key role in systemic acquired resistance (Wildermuth et al., 2001). *PAL* has been previously shown to be induced in wheat during defence against *Z. tritici* (Rudd et al., 2015; Shetty et al., 2009) and more recently systemic changes in metabolites of PAL, including lignin, were demonstrated (Seybold et al., 2020). Indeed, our results also show that *PAL* expression correlated with lignin accumulation in both genotypes, with lignification being observed first in the resistant genotype. In the present study, the SA-marker genes *PR1* and *PR5* correlated with levels of endogenous SA in Sacramento at 8 hpi but were inversely related to anthocyanins or lignification, suggesting that SA biosynthesis may have been favoured. In contrast, at 8 hpi in Cougar, *ICS* was down-regulated, suggesting suppression of SA biosynthesis via this pathway whilst *PAL* remained up-regulated together with a significant increase of anthocyanins from 4 to 24 hpi, suggesting that secondary metabolites rather than SA contributed to the response to *Z. tritici*. Furthermore, in Cougar, the observed up-regulation of JA biosynthesis genes together with JA in opposition to SA and SA-induced gene expression demonstrate that the JA signalling pathway contributed to defence against *Z. tritici* in the resistant genotype.

In conclusion, ABA synthesis positively associated with JA and in antagonistic action to SA-dependent responses contributed to the early defence against *Z. tritici* in Cougar, characterized by the lack of HR and effective ROS regulation in the chloroplast. In contrast, the SA-induced response and oxidative stress in the compatible interaction with Sacramento benefited disease progression by *Z. tritici*, resulting in a photosynthetic trade-off cost of shutdown of photosynthesis and stomatal conductance at 5 dpi before symptom expression.

ACKNOWLEDGEMENTS

We thank Andrew Lee (University of Nottingham) and Dr Petra Ungerer (Queen Mary, University of London) for technical assistance. This work was carried out under the Capture project supported by Innovate UK (grant no. 38936-273309) and the Biotechnology and Biological Sciences Research Council (grant no. BB/M011550/1), led by Agrii in collaboration with RAGT Seeds.

AUTHOR CONTRIBUTIONS

O.O.A., D.P.J., A.V.R., E.H.M., R.S., and R.V.R. designed the research; O.O.A., D.P.J., and D.A. performed the experiments; V.P. performed phytohormone analysis; O.O.A., D.P.J., and R.V.R. analysed data; O.O.A., D.P.J., and R.V.R. wrote the manuscript.

DATA AVAILABILITY STATEMENT

The data that support the findings of this study are available from the corresponding author upon reasonable request.

ORCID

Rumiana V. Ray https://orcid.org/0000-0003-3510-1090

REFERENCES

Alscher, R.G., Erturk, N. & Heath, L.S. (2002) Role of superoxide dismutases (SODs) in controlling oxidative stress in plants. *Journal of Experimental Botany*, *53*, 1331–1341.

Apel, K. & Hirt, H. (2004) Reactive oxygen species: metabolism, oxidative stress, and signal transduction. *Annual Review of Plant Biology*, *55*, 373–399.

Chater, C.C.C., Oliver, J., Casson, S. & Gray, J.E. (2014) Putting the brakes on: abscisic acid as a central environmental regulator of stomatal development. *New Phytologist*, *202*, 376–391.

Chernys, J.T. & Zeevaart, J.A.D. (2000) Characterization of the 9-*cis*-epoxycarotenoid dioxygenase gene family and the regulation of abscisic acid biosynthesis in avocado. *Plant Physiology*, *124*, 343–354.

Chirinos, R., Campos, D., Arbizu, C., Rogez, H., Rees, J.-F., Larondelle, Y. et al. (2007) Effect of genotype, maturity stage and post-harvest storage on phenolic compounds, carotenoid content and antioxidant capacity, of Andean mashua tubers (*Tropaeolum tuberosum* Ruiz and Pavón). *Journal of the Science of Food and Agriculture*, *87*, 437–446.

Choi, Y.E., Lee, C. & Goodwin, S.B. (2016) Generation of reactive oxygen species via NOXa is important for development and pathogenicity of *Mycosphaerella graminicola*. *Mycobiology*, *44*, 38–47.

Davison, P.A., Hunter, C.N. & Horton, P. (2002) Overexpression of β-carotene hydroxylase enhances stress tolerance in *Arabidopsis*. *Nature*, *418*, 203–206.

Demmig-Adams, B. & Adams, W.W. (2006) Photoprotection in an ecological context: The remarkable complexity of thermal energy dissipation. *New Phytologist*, *172*, 11–21.

Demmig-Adams, B., Cohu, C.M., Amiard, V., Zadelhoff, G., Veldink, G.A., Muller, O. et al. (2013) Emerging trade-offs – impact of photoprotectants (PsbS, xanthophylls, and vitamin E) on oxylipins as regulators of development and defense. *New Phytologist*, *197*, 720–729.

Faralli, M., Matthews, J. & Lawson, T. (2019) Exploiting natural variation and genetic manipulation of stomatal conductance for crop improvement. *Current Opinion in Plant Biology*, *49*, 1–7.

Färber, A., Young, A.J., Ruban, A.V., Horton, P. & Jahns, P. (1997) Dynamics of xanthophyll-cycle activity in different antenna subcomplexes in the photosynthetic membranes of higher plants (The relationship between zeaxanthin conversion and nonphotochemical fluorescence quenching). *Plant Physiology*, *115*, 1609–1618.

Foyer, C.H. & Noctor, G. (2005) Oxidant and antioxidant signaling in plants: A re-evaluation of the concept of oxidative stress in a physiological context. *Plant, Cell and Environment*, *28*, 1056–1071.

Gamir, J., Pastor, V., Cerezo, M. & Flors, V. (2012) Identification of indole-3-carboxylic acid as mediator of priming against *Plectosphaerella cucumerina*. *Plant Physiology and Biochemistry*, *61*, 169–179.

Göhre, V., Jones, A.M.E., Sklenář, J., Robatzek, S. & Weber, A.P.M. (2012) Molecular crosstalk between PAMP-triggered immunity and photosynthesis. *Molecular Plant-Microbe Interactions*, *25*, 1083–1092.

Govrin, E.M. & Levine, A. (2000) The hypersensitive response facilitates plant infection by the necrotrophic pathogen *Botrytis cinerea*. *Current Biology*, *10*, 751–757.

Huang, J., Gu, M., Lai, Z., Fan, B., Shi, K., Zhou, Y.-H. et al. (2010) Functional analysis of the *Arabidopsis PAL* gene family in plant growth, development, and response to environmental stress. *Plant Physiology*, *153*, 1526–1538.

Kema, G.H.J., Yu, D.Z., Rijkenberg, F.H.J., Shaw, M.W. & Baayen, R.P. (1996) Histology of the pathogenesis of *Mycosphaerella graminicola* in wheat. *Phytopathology*, *86*, 777–786.

Kettles, G.J. & Kanyuka, K. (2016) Dissecting the molecular interactions between wheat and the fungal pathogen *Zymoseptoria tritici*. *Frontiers in Plant Science*, *7*, 508.

Lee, W., Hammond-Kosack, K.E., Rudd, J.J., Kanyuka, K. & Devonshire, B.J. (2015) Deregulation of plant cell death through disruption of chloroplast functionality affects asexual sporulation of *Zymoseptoria tritici* on wheat. *Molecular Plant-Microbe Interactions*, *28*, 590–604.

Li, N., Han, X., Feng, D., Yuan, D. & Huang, L.J. (2019) Signaling crosstalk between salicylic acid and ethylene/jasmonate in plant defense: do we understand what they are whispering? *International Journal of Molecular Sciences*, *20*, 671.

Murchie, E.H. & Ruban, A.V. (2020) Dynamic non-photochemical quenching in plants: from molecular mechanism to productivity. *The Plant Journal*, *101*, 885–896.

Pastor, V., Sánchez-Bel, P., Gamir, J., Pozo, M.J. & Flors, V. (2018) Accurate and easy method for systemin quantification and examining metabolic changes under different endogenous levels. *Plant Methods*, *14*, 33.

Pastori, G.M., Kiddle, G., Antoniw, J., Bernard, S., Veljovic-Jovanovic, S., Verrier, P.J. et al. (2003) Leaf vitamin C contents modulate plant defense transcripts and regulate genes that control development through hormone signaling. *The Plant Cell*, *15*, 939–951.

Ray, R.V., Jenkinson, P. & Edwards, S.G. (2004) Effects of fungicides on eyespot, caused predominantly by *Oculimacula acuformis*, and yield of early-drilled winter wheat. *Crop Protection*, *23*, 1199–1207.

Ruban, A.V. (2016) Nonphotochemical chlorophyll fluorescence quenching: Mechanism and effectiveness in protecting plants from photodamage. *Plant Physiology*, *170*, 1903–1916.

Rubiales, D. & Niks, R.E. (1996) Avoidance of rust infection by some genotypes of *Hordeum chilense* due to their relative inability to induce

the formation of appressoria. *Physiological and Molecular Plant Pathology*, *49*, 89–101.
Rudd, J.J., Kanyuka, K., Hassani-Pak, K., Derbyshire, M., Andongabo, A., Devonshire, J. et al. (2015) Transcriptome and metabolite profiling of the infection cycle of *Zymoseptoria tritici* on wheat reveals a biphasic interaction with plant immunity involving differential pathogen chromosomal contributions and a variation on the hemibiotrophic lifestyle definition. *Plant Physiology*, *167*, 1158–1185.
Serrano, I., Audran, C. & Rivas, S. (2016) Chloroplasts at work during plant innate immunity. *Journal of Experimental Botany*, *67*, 3845–3854.
Seybold, H., Demetrowitsch, T.J., Hassani, M.A., Szymczak, S., Reim, E., Haueisen, J. et al. (2020) A fungal pathogen induces systemic susceptibility and systemic shifts in wheat metabolome and microbiome composition. *Nature Communications*, *11*, 1910.
Shetty, N.P., Jensen, J.D., Knudsen, A., Finnie, C., Geshi, N., Blennow, A. et al. (2009) Effects of β-1,3-glucan from *Septoria tritici* on structural defence responses in wheat. *Journal of Experimental Botany*, *60*, 4287–4300.
Shetty, N.P., Kristensen, B.K., Newmana, M.A., Møller, K., Gregersen, P.L. & Jørgensen, H.J.L. (2003) Association of hydrogen peroxide with restriction of *Septoria tritici* in resistant wheat. *Physiological and Molecular Plant Pathology*, *62*, 333–346.
Steyn, W.J., Wand, S.J.E., Holcroft, D.M. & Jacobs, G. (2002) Anthocyanins in vegetative tissues: A proposed unified function in photoprotection. *New Phytologist*, *155*, 349–361.
Tateda, C., Obara, K., Abe, Y., Sekine, R., Nekoduka, S., Hikage, T. et al. (2019) The host stomatal density determines resistance to *Septoria gentianae* in Japanese gentian. *Molecular Plant-Microbe Interactions*, *32*, 428–436.
Ton, J., Flors, V. & Mauch-Mani, B. (2009) The multifaceted role of ABA in disease resistance. *Trends in Plant Science*, *14*, 310–317.
de Torres Zabala, M., Littlejohn, G., Jayaraman, S., Studholme, D., Bailey, T., Lawson, T. et al. (2015) Chloroplasts play a central role in plant defence and are targeted by pathogen effectors. *Nature Plants*, *1*, 15074.
Triantaphylidès, C., Krischke, M., Hoeberichts, F.A., Ksas, B., Gresser, G., Havaux, M. et al. (2008) Singlet oxygen is the major reactive oxygen species involved in photooxidative damage to plants. *Plant Physiology*, *148*, 960–968.
Vicente, J., Mendiondo, G.M., Pauwels, J., Pastor, V., Izquierdo, Y., Naumann, C. et al. (2019) Distinct branches of the N-end rule pathway modulate the plant immune response. *New Phytologist*, *221*, 988–1000.
Walker, G.M. & White, N.A. (2017) Introduction to fungal physiology. In: Kavanagh, K. (Ed.) *Fungi: Biology and Applications*. Wiley, pp. 1–35.
Wang, M., Wang, Y., Wu, H., Xu, J., Li, T., Hegebarth, D. et al. (2016) Three *TaFAR* genes function in the biosynthesis of primary alcohols and the response to abiotic stresses in *Triticum aestivum*. *Scientific Reports*, *6*, 25008.
Wildermuth, M.C., Dewdney, J., Wu, G. & Ausubel, F.M. (2001) Isochorismate synthase is required to synthesize salicylic acid for plant defence. *Nature*, *414*, 562–565.
Zhang, X. & Liu, C.-J. (2015) Multifaceted regulations of gateway enzyme phenylalanine ammonia-lyase in the biosynthesis of phenylpropanoids. *Molecular Plant*, *8*, 17–27.
Ziv, C., Zhao, Z., Gao, Y.G. & Xia, Y. (2018) Multifunctional roles of plant cuticle during plant–pathogen interactions. *Frontiers in Plant Science*, *9*, 1088.

SUPPORTING INFORMATION

Additional supporting information may be found online in the Supporting Information section.

How to cite this article: Ajigboye OO, Jayaweera DP, Angelopoulou D, et al. The role of photoprotection in defence of two wheat genotypes against *Zymoseptoria tritici*. *Plant Pathol*. 2021;00:1–15. https://doi.org/10.1111/ppa.13392